Headline Articles

Study of the Electronic Structure of GaAs(100) Single Crystal Electrode/Electrolyte Interfaces by Electrochemical Tunneling Spectroscopy

Kohei Uosaki,* Shen Ye, and Namiki Sekine

Physical Chemistry Laboratory, Division of Chemistry, Graduate School of Science, Hokkaido University, Sapporo 060

(Received September 28, 1995)

An electrochemical tunneling spectroscopy (ETS) system is constructed to study the electronic structure of semiconductor/electrolyte interfaces. By using this system, the tunneling current of GaAs (100) single crystal electrodes in solution was measured as a function of electrode potential at a constant sample-tip distance. Tunneling current flowed in the forward bias region; the current depended on the bias, i.e., the potential with respect to the flat band potential. It decreased by decreasing the bias and became zero near the flat band potential. This behavior can be explained by considering the potential dependence of the surface concentration of the majority carriers. The space charge layer within the semiconductor formed in the reverse bias region worked as an extra barrier for the tunneling process; therefore, no tunneling current was observed in this potential region. Current in the direction opposite to that in the forward bias region flowed as the reverse bias became very large, although this current was very small. In this potential region, the thickness of the space charge layer near the Fermi level of the tip became thinner and electrons were able to tunnel through the barrier. Effects of the doping density, the tip potential, the pre-set tunneling current and the initial sample potential as well as the surface treatment on the tunneling current–electrode potential relation were investigated in detail at n-GaAs(100) single crystal electrodes. The tunneling behaviors in the forward and reverse bias regions were discussed semi-quantitatively based on the calculation of surface electron concentration and the transmission coefficient through the space charge barrier, respectively.

Because most surface science techniques, such as LEED, XPS, and IR, can only provide information averaged over a wide region of the surface, it had been difficult to study the properties of local surface regions (~nm) until the scanning tunneling microscope (STM) was invented by Binnig and Rohrer in 1982.[1,2] Because a tunneling current flows through a region only several nm square, STM can provide information about a solid surface with a very high spatial resolution. STM now becomes a routine technique to obtain the information about morphological structures of solid surface on an atomic scale in ultra high vacuum (UHV), in air, or even in an electrolyte solution. The applications and the theory of the STM have been reviewed extensively.[3—7]

As tunneling current depends on the overlap between the wave functions of sample and tip and is proportional to the local density of states (LDOS) of the sample with an s-wave (free electron) metal tip, STM can be used to obtain not only the topographic information of the surface but also the information about the electronic structure of the sample surface on an atomic scale (scanning tunneling spectroscopy: STS). In fact, the STM was initially designed for this purpose.[1]

STS has been successfully applied for the studies of electronic structures of metals and semiconductors in UHV[8—17] and in air.[18—22] Hamers et al. reported an atomically resolved electronic structure of the Si(111)(7×7) surface obtained by STS measurement in UHV for the first time.[8,9] In addition to a conventional image, they mapped out the complete electronic structure of a Si(111)(7×7) unit cell. The results are in good agreement with previous results obtained by spectroscopic measurements for large areas such as ultraviolet photoemission spectroscopy (UPS) and inverse photoemission spectroscopy (IPS). Bard et al. carried out the tunneling spectroscopy (TS) measurement on an n-FeS_2(001) semiconductor in air.[18] They observed a peak at 1.6 eV from the Fermi level in the normalized conductance spectrum; this peak is attributed to the valence level consisting mainly of Fe3dt_{2g} states of the sample.

The information of the electronic structure of semiconductor/electrolyte interface, such as the band position, band bending and the position and the density of the surface states, is very important in semiconductor electrochemistry.[23] Many techniques are available to obtain such information. We have

demonstrated that photoluminescence (PL) and electroluminescence (EL) measurements are useful to obtain such information to understand the photoelectrochemical processes at semiconductor electrodes. For example, PL measurements showed that the surface recombination rate at p-GaAs electrode is increased by the surface Pt modification.[24] EL measurements proved the formation of the inversion layer at p-GaAs[25] and the accumulation layer at n-GaAs[26] and the existence of the intermediate adsorbed hydrogen at p-GaAs surface.[27]

The information on the local morphological structure and electronic states is essential to understand fully the surface reactivity of electrodes. STM and atomic force microscope (AFM) have been employed successfully to observe surface structures of semiconductor electrodes in electrolyte solution under potential control on atomic scale.[28—35] STS measurement is expected to provide much valuable information about the local electronic structure of an electrode in electrolyte solution. However, reports of electrochemical STS or even tunneling spectroscopic (TS) study on electrodes in electrolyte solution are very limited. Although several papers on TS measurements on metal electrodes have been published,[36,37] the results are still only preliminary. No real STS or TS study with the controlled tip-sample distance has been carried out on semiconductor electrodes.

Itaya et al. reported that the STM measurement of TiO_2 and ZnO electrode was possible only when the electrode potential was more negative than the flat band potential (V_{fb}), i.e., in the forward bias region.[38,39] The tip touched the electrode surface when the electrode was in the depletion condition.

We have shown that the measurement of the tip current as a function of the potential of the semiconductor electrode in solution, with the feedback circuit of STM active, provides the information of the electronic structure of semiconductor surface and named this method as tip-current voltammetry (TCV).[40—43] The pre-set tunneling current flowed at the STM tip on the etched surface of n-GaAs when the potential was more negative than the V_{fb}. It flowed even when the potential was more positive than the V_{fb}, although there existed the space charge region within the semiconductor. As potential was made more positive, tip current started to decrease and finally became zero and the tip touched the semiconductor surface. As the potential became much more positive, the tip was removed from the n-GaAs surface and the tip current began to increase. The tip current finally reached the pre-set value. The reverse situation was observed at the p-GaP electrode. The detailed studies including the effects of the surface treatment suggest that the tip current (i_T)–electrode potential (V) relations were strongly affected by the density of the surface states. Actually, the i_T–V relation at the n-GaAs electrode treated with sulfur, which is known to reduce the density of surface states,[44] showed an ideal diode-like behavior: i_T became zero at the V_{fb} and no i_T was observed in the potential region more positive than the V_{fb}. Because a commercial STM unit with a feedback circuit active was used in the TCV, the sample-tip distance changed during the measurement and the tip touched the semiconductor electrode surface in the potential region where i_T is less than the pre-set tunneling current. To probe the electronic structure at the electrode/electrolyte interface in more well-defined surface conditions of both sample and tip, one needs to measure i_T as a function of the electrode potential with a fixed tip-sample distance.

We have constructed a new system by which the tunneling current can be measured as a function of the potential of both sample and tip under a constant sample-tip distance or as a function of the sample-tip distance under constant potentials of sample and tip. One may call this electrochemical tunneling spectroscopy (ETS). By using the system, we measured i_T–V relations of n-GaAs and p-GaAs. Effects of doping density, tip potential, the pre-set potential/current, surface treatment on the i_T–V characteristics were investigated in detail. We analyzed the results qualitatively and semi-quantitatively and compared them with the results of TCV.

Experimental

Construction of ETS System. In order to carry out the TS measurement under a constant sample-tip distance, the STM feedback loop must be cut and the piezo voltage of the tip must be controlled externally. A NanoScope I (Digital Instruments) was modified to carry out the electrochemical tunneling spectroscopy (ETS) measurement. The block diagram of the system is shown in Fig. 1. An analog switch and a sample hold (S/H) circuit were inserted into the feedback circuit of NanoScope I. The switch, which is controlled by a personal computer (PC9801RA5, NEC), selects the input to the S/H circuit between the feedback loop and the output of a D/A converter. The switching rate was ca. 2 μs. In the case of ordinary STM, i.e., internal feedback control mode, the piezo voltage of the tip was controlled by the STM feedback circuit and the tunneling current and piezo voltage of the tip were monitored by the computer via an external 16 bit A/D converter (ADM1698-BPC, MicroScience); the bias was controlled by the computer via an external 16 bit D/A converter (TDA-2698XPC, MicroScience). After the tip was brought close to the surface and a stable tunneling state was achieved, the feedback loop was cut by the switch and voltage measured by the S/H circuit was applied to the Z-piezo by the D/A converter (external mode). In the case of external control mode, the tip-sample distance can be controlled by changing the Z-piezo voltage applied to the tip. The tunneling current can be measured as a function of bias under a constant tip-sample distance or as a function of tip-sample distance under a constant bias.

The pre-amplifier in NanoScope I converts the tunneling current into voltage by employing a 1 MΩ resistor between the tip and the ground (Fig. 1).[45] In this arrangement, the actual bias (ΔV) applied to the tip-sample differs from the pre-set bias ($\Delta V_{pre\text{-}set}$) and is given by:

$$\Delta V = V_{pre\text{-}set} - i_T R, \quad (1)$$

where i_T is the tunneling current and R=1 (MΩ). Thus ΔV depends on the tunneling current and this makes a serious error in the bias value when the tunneling current is large. We corrected this error by adding $i_T R$ to the $\Delta V_{pre\text{-}set}$ through a D/A converter. Two resistors in the setpoint circuit of NanoScope I were replaced so that the maximum tunneling current which could be measured was expanded from the standard value of 10 nA to 100 nA.[45]

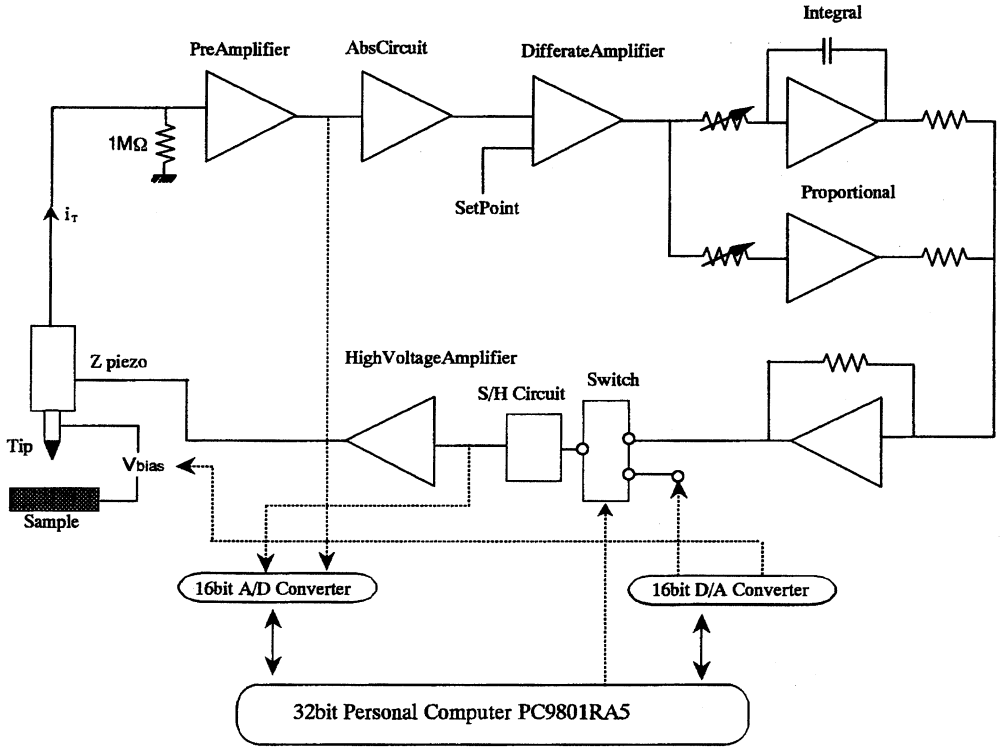

Fig. 1. A block diagram for the TS experiment.

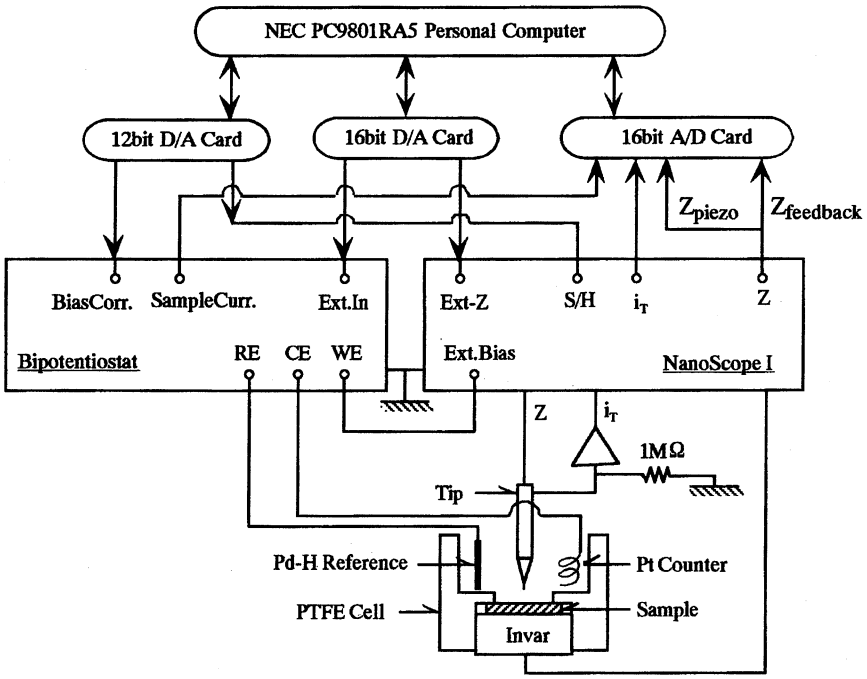

Fig. 2. Experimental arrangement for the ETS measurement with an electrochemical cell and a bipotentiostat.

The block diagram for the electrochemical tunneling spectroscopy (ETS) system is shown in Fig. 2. The potentials of the sample and the tip were controlled by a home-built bipotentiostat.[46] The reference electrode was a Pd–H electrode charged sufficiently before each measurement at a current density of 10 $\mu A\,cm^{-2}$. The potential of the Pd–H electrode was corrected by recording the cyclic voltammogram of platinum electrode in the same solution by using the Pd–H as a reference electrode just after the ETS experiment. All the potentials in this paper were referred to reversible hydrogen electrode (RHE) scale. The counter electrode was a Pt wire. The electrochemical cell made from PTFE was screwed onto an invar metal plate and the plate was fixed onto the STM micro-

scope stage by a magnet. The tip was a simply cut Pt wire (0.3 mm) insulated with apiezon wax. The electrolyte solution, 2 mM $HClO_4$ (pH=2.77), was deaerated by bubbling N_2 through the solution before each measurement.

Materials. Four kinds of semiconductor electrodes were used in this study: one of them was Zn doped p-GaAs single crystal with the (100) face exposed ($N_A=1.01\times10^{19}$ cm^{-3}), and three of them were Si doped n-GaAs single crystals with the (100) face exposed with various doping densities ($N_D=0.84\times10^{18}$, 2.48×10^{18}, and 4.2—8.0×10^{18} cm^{-3}). The ohmic contact was obtained by soldering with In/Zn alloy on p-GaAs and with In on n-GaAs. Prior to the ETS measurement, the electrodes were etched with $H_2O:H_2O_2:H_2SO_4$ solution (1 : 1 : 4) for 30 s, then, rinsed with Milli-Q water and finally dried blowing nitrogen.

The surface modification by ruthenium was carried out by dipping the etched electrode in $RuCl_3$ solution (1 g of $RuCl_3\cdot nH_2O$ in 10 cm^3 water) for 30 min, followed by thorough rinsing with Milli-Q water.[47] The surface modification by sulfur was carried out by immersing the etched electrode overnight in an aqueous solution of $(NH_4)_2S$ with excess S, followed by thorough rinsing with Milli-Q water.[44]

Results

Figure 3A and 3B show the typical i_T–V relations at n-GaAs ($N_D=0.84\times10^{18}$ cm^{-3}) and p-GaAs electrodes, respectively, obtained as follows. The sample potential was first set in the forward region (−0.54 V for n-GaAs in Fig. 3A and +0.47 V for p-GaAs in Fig. 3B) and the tip (Pt) potential was set in the double layer region of Pt (+0.24 V in Fig. 3A and +0.37 V in Fig. 3B). Pre-set tunneling currents for n-GaAs and p-GaAs were −5 nA and 8 nA, respectively. In this paper, electron tunneling from the sample to the tip was denoted as cathodic current and from the tip to the sample as anodic current. The tip was approached to the sample surface and a tunneling state was achieved under ordinary STM feedback control. The STM was then switched into the external control mode and the potential of GaAs electrode was swept while the tip potential and the tip-sample distance were kept constant. The scan rate was ca. 0.28 V s^{-1}. All the results presented in this work were obtained in this manner, although various parameters including pre-set initial sample potential, pre-set tunneling current and tip potential were varied.

In both cases, tunneling current decreased quickly as forward bias decreased and only very small tunneling currents flowed at potentials more positive than ca. −0.35 V at n-GaAs electrode (Fig. 3A) or more negative than +0.3 V at p-GaAs electrode (Fig. 3B). A tunneling current of reverse direction was observed at n-GaAs electrode at much more positive potential region, ca. >+2 V (Fig. 3A) or at p-GaAs electrode at much more negative potential region, ca. <−0.1 V (Fig. 3B).

In the following sections, effects of various parameters on the tunneling behavior will be described. An anodic dissolution current flowed in forward bias at p-GaAs; due to this, changes in surface nature were expected during ETS measurement. Thus, detailed study was carried out by using n-GaAs electrodes only.

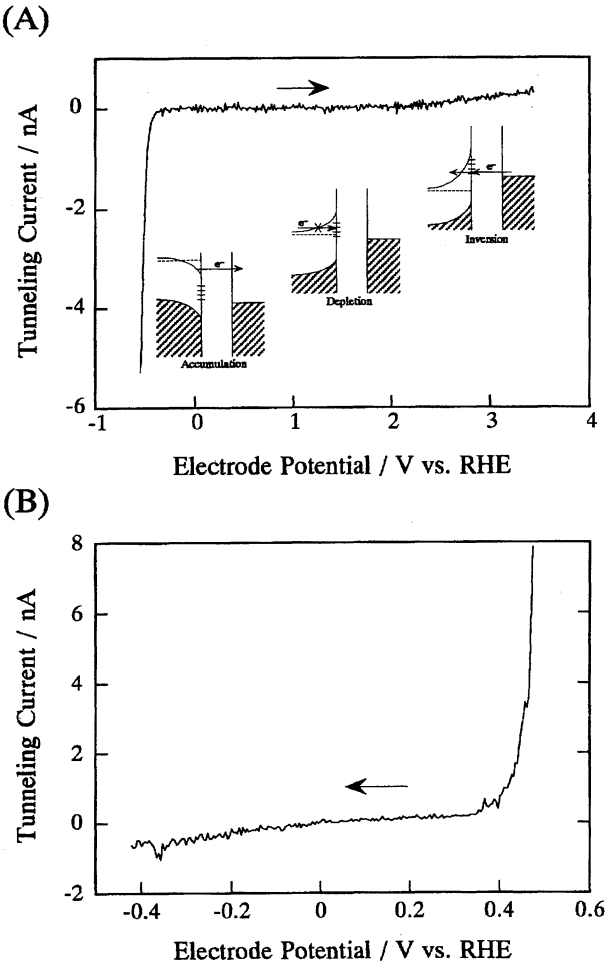

Fig. 3. Typical results of ETS measurements at (A) n-GaAs ($N_D=0.84\times10^{18}$ cm^{-3}); (B) p-GaAs ($N_A=1.01\times10^{19}$ cm^{-3}) electrodes in 2 mM $HClO_4$ solution (1 M=1 mol dm^{-3}).

Effect of Doping Density. Figure 4 shows i_T–V relations of n-GaAs electrodes of various doping densities. The initial potential of n-GaAs electrode was set at −0.45 V in forward region and the tip potential was set at +0.16 V. Although we employed the same initial n-GaAs electrode potential with respect to Pd–H reference electrode, the potential of Pd–H reference electrode with respect to RHE differed between experiments, and, therefore, the initial potential in the figure presented with respect to RHE differed slightly from one experiment to another. After a −5 nA pre-set current was attained under STM internal feedback control mode, the external control mode was activated and the potential of n-GaAs electrode was swept into positive direction to record the i_T–V relation with a constant tip potential. The cathodic tunneling current decreased quickly as the electrode potential was made positive. The tunneling current decreased to zero around ca. −0.2 V (curve a for $N_D=0.84\times10^{18}$ cm^{-3} and curve b for $N_D=2.48\times10^{18}$ cm^{-3} in Fig. 4A). No current was observed when the potential became more positive than ca. −0.2 V. A small anodic current, however, flowed in the very positive potential region, as shown in Fig. 4B. The

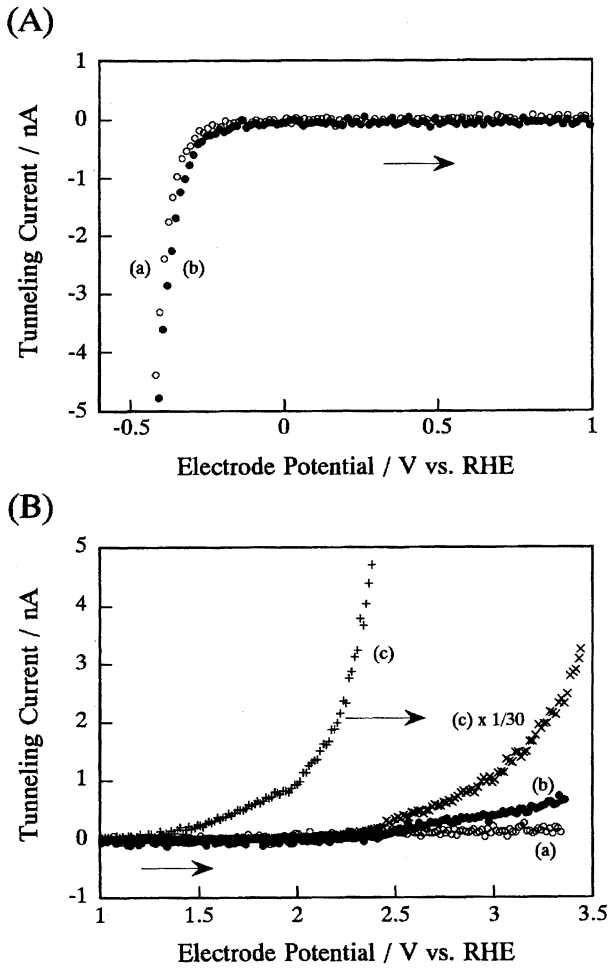

Fig. 4. Effect of doping density on ETS behavior of n-GaAs electrode: (a) 0.84×10^{18} cm^{-3}; (b) 2.48×10^{18} cm^{-3}; (c) 4.2—8.0×10^{18} cm^{-3} in (A) cathodic (B) anodic regions.

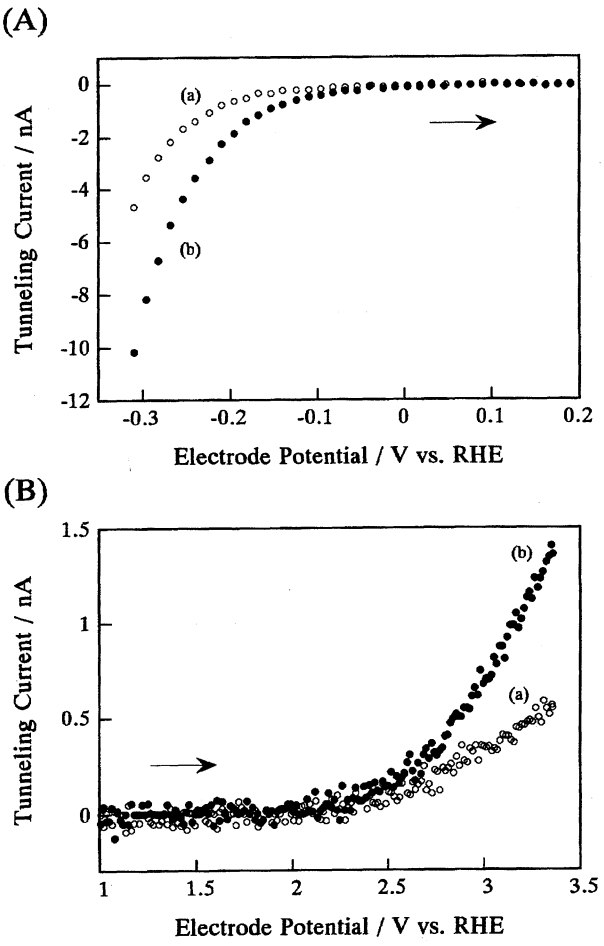

Fig. 5. Effect of pre-set tunneling current on ETS behavior of n-GaAs electrode ($N_D=2.48\times10^{18}$ cm^{-3}) for (A) cathodic and (B) anodic regions. The pre-set tunneling current were (a) −4.5 nA and (b) −10 nA. The tip potential was +0.36 V and the potential of n-GaAs electrode was −0.31 V.

amount of the current in this region depended on the doping density very much. The anodic tunneling current was smaller at the n-GaAs electrode of lower doping density and no current flowed until the potential became more positive than +2.5 V (curve a for $N_D=0.84\times10^{18}$ and curve b for 2.48×10^{18} cm^{-3}). On the other hand, the current began to flow at n-GaAs electrode of highest doping density even from +1.2 V (curve c for $N_D=4.2$—8.0×10^{18} cm^{-3} in Fig. 4B). The anodic currents at +3.3 V were 0.2 nA, 0.8 nA, and 100 nA (Fig. 4B) for n-GaAs of lowest, medium, and highest doping densities, respectively.

Effect of Pre-Set Current. Figure 5 shows i_T–V relations of a n-GaAs electrode ($N_D=2.48\times10^{18}$ cm^{-3}) in forward (Fig. 5A) and reverse bias region (Fig. 5B), obtained with the different pre-set tunneling currents (a) −4.5 nA and (b) −10 nA. The initial tip and sample potentials were +0.36 V and −0.31 V, respectively. In the forward bias region, the tunneling current at a given potential was larger at an n-GaAs electrode with a larger pre-set current. For example, the currents at −0.25 V were −1.8 nA and −4.0 nA for pre-set currents of −4.5 nA and −10 nA, respectively. As the potential was made more positive, the tunneling current decreased. The apparent potential dependence of the tunneling current is a strong function of the pre-set current. The larger the pre-set current, the faster the tunneling current decreased with potential. In the reverse bias region, anodic tunneling current at a give potential was smaller with smaller pre-set current (Fig. 5B). For example, the currents at +3.2 V were 0.5 nA and 1.1 nA for pre-set currents of −4.5 nA and −10 nA, respectively (Fig. 5B).

Effect of Initial Sample Potential. Figure 6 shows i_T–V relations of a n-GaAs electrode ($N_D=0.84\times10^{18}$ cm^{-3}) for forward (Fig. 6A) and reverse bias regions (Fig. 6B) obtained with different initial sample potentials. The initial sample potential was pre-set to −0.55 V for curve a and −0.45 V for curve b. The tip whose potential was +0.15 V was brought close to the sample surface and a stable tunneling current (−5 nA) was achieved in the forward bias region under the STM internal feedback control mode. In the forward bias region, the cathodic tunneling current decreased with the potential at nearly the same rate. At a given electrode potential, the

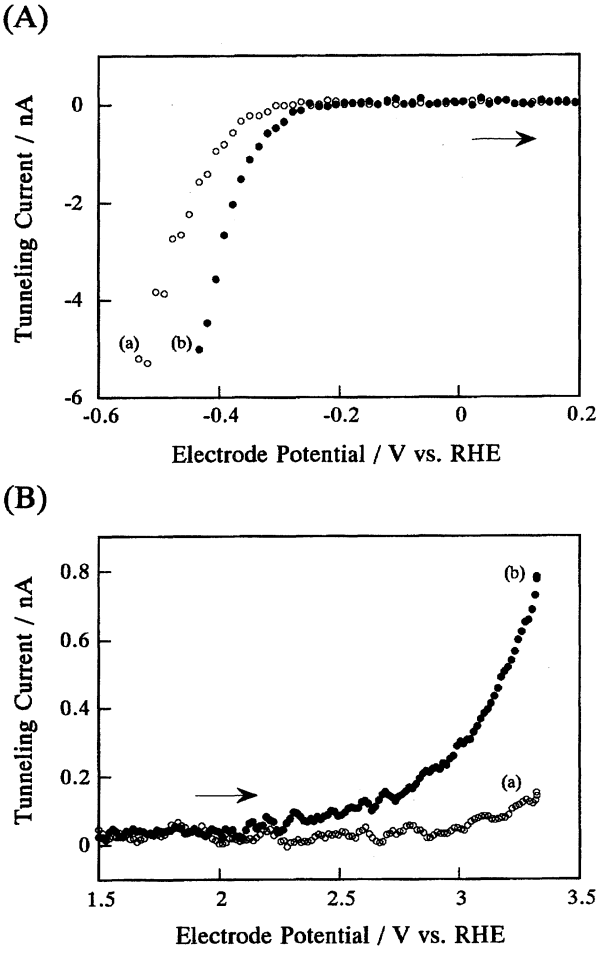

Fig. 6. Effect of initial sample potential on ETS behavior of n-GaAs electrode (N_D=2.48×10^{18} cm^{-3}) for (A) cathodic and (B) anodic regions. The n-GaAs sample potential were (a) −0.55 V and (b) −0.45 V. The tip potential was +0.15 V and the pre-set tunneling current was −5 nA.

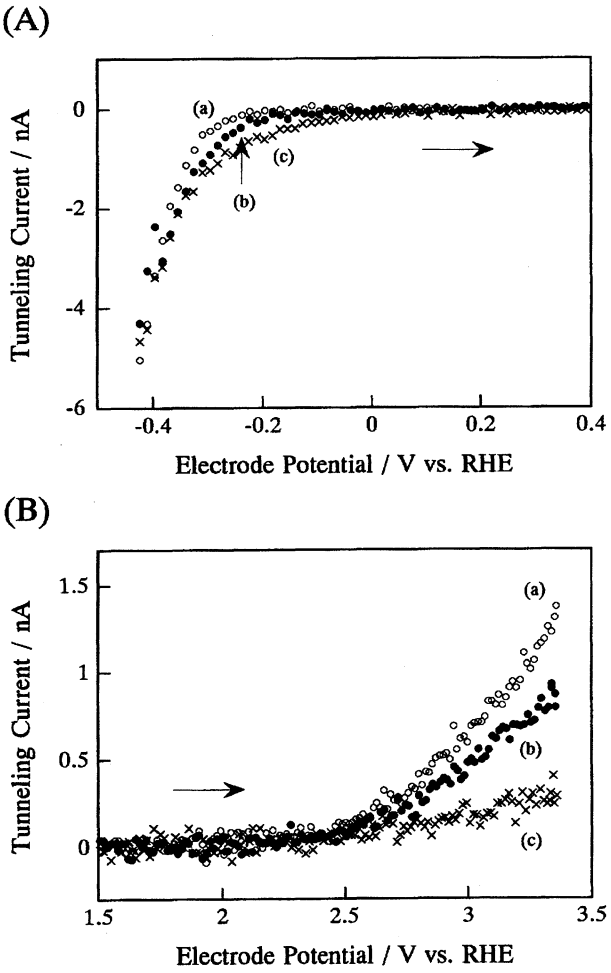

Fig. 7. Effect of tip potential on ETS behavior of n-GaAs electrode (N_D=2.48×10^{18} cm^{-3}) in (A) cathodic and (B) anodic regions. The tip potential (a) +0.16 V, (b) +0.36 V, and (c) +0.56 V. Initial sample potential was −0.42 V and pre-set current was −5 nA.

cathodic current was larger for curve b than for curve a. For example, currents at −0.4 V were ca. −1 nA and −4 nA for the initial potentials of −0.55 V and −0.45 V, respectively (Fig. 6A). The tunneling current became zero at −0.2 V and no current was observed at a potential more negative than +2 V in either case. A small anodic tunneling current flowed at potentials more positive than +2 V. The more positive the pre-set sample potential was, the more easily the anodic tunneling current flowed. The anodic tunneling current at +3.2 V with initial sample potential of −0.45 V was 5 times larger than that of −0.55 V (Fig. 6B).

Effect of Tip Potential. Figure 7 shows i_T–V relations of a n-GaAs electrode (N_D=2.48×10^{18} cm^{-3}) obtained with different tip potentials: (a) +0.16 V, (b) +0.36 V, and (c) +0.56 V. The initial sample potential was −0.42 V and the pre-set tunneling current was −5 nA. The sample potential was swept from −0.42 V to +3.3 V. In the forward bias region (Fig. 7A), the tunneling current flowed more easily at more positive tip potentials. For example, the currents at −0.3 V were ca. −0.5 nA, −1.1 nA, and −1.3 nA for the tip potentials of +0.16 V, +0.36 V, and +0.56 V, respectively. In the reverse bias region (Fig. 7B), no tunneling current was observed in the potential region more negative than +2.5 V. When the potential of n-GaAs electrode became more positive than +2.5 V, a small anodic tunneling current was observed. At a given n-GaAs electrode potential, the more negative the tip potential was, the larger the anodic tunneling current which flowed. For example, the anodic tunneling currents at +3.2 V were 1.0 nA, 0.6 nA, and 0.1 nA for the tip potentials of +0.16 V, +0.36 V, and +0.56 V, respectively.

Effect of Surface Treatments. To clarify the role of the surface state on the i_T–V relation, we have modified the n-GaAs surface with the ruthenium and sulfur. Ruthenium and sulfur are known to increase and decrease the surface state density on GaAs surface, respectively.[24,27,46,47] The significant effects of surface treatment by ruthenium and sulfur on the tip current-potential relation at GaAs electrode with STM feedback circuit active (TCV) have been demonstrated previously.[40–43]

After the surface modification, i_T–V relations were measured with the pre-set tunneling current of −5 nA. The initial n-GaAs potential was −0.30 V and the tip potential was +0.44 V.

Figure 8A shows the i_T–V relation of a n-GaAs electrode (N_D=0.84×10^{18} cm^{-3}) with (a) usual etching treatment and (b) Ru treatment. The tunneling current in the forward bias region was nearly the same at etched and Ru treated electrodes. On the other hand, the anodic tunneling current was much larger at Ru treated n-GaAs electrode than at the etched electrode in the reverse bias region. The anodic current began to flow at ca. +1.3 V at the Ru-treated surface, which is much more negative than the value at the etched surface (+2.5 V).

Figure 8B shows the i_T–V relation of (a) etched and (b) S-treated n-GaAs electrodes of highest doping density (N_D=4.2—8.0×10^{18} cm^{-3}). While no obvious effect was observed in the forward bias region, a significant effect of the S modification was observed in the reverse bias region.

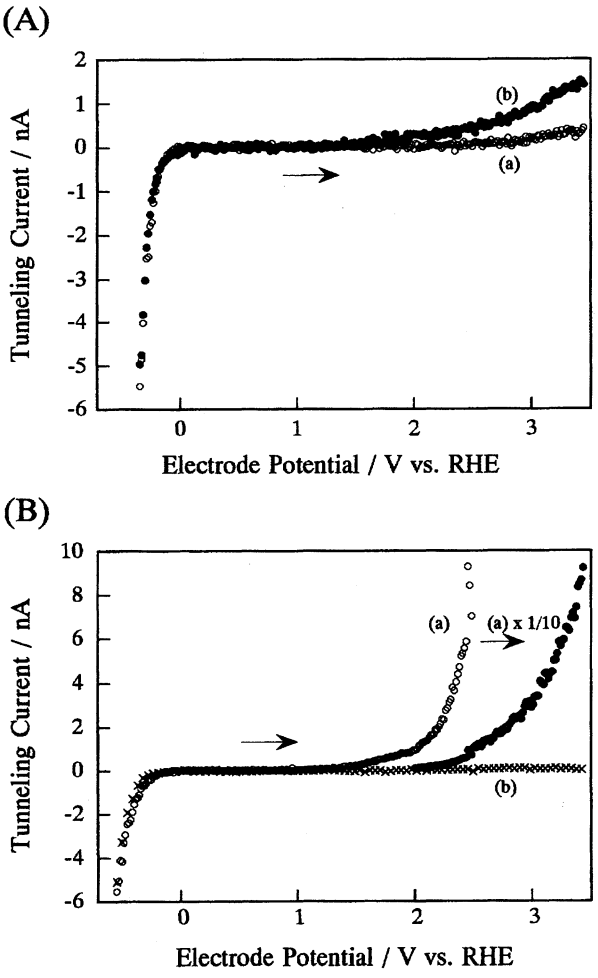

Fig. 8. (A) i_T–V relations of (a) etched and (b) Ru-treated n-GaAs electrode (N_D=0.84×10^{18} cm^{-3}). (B) i_T–V relations of (a) etched and (b) S-treated n-GaAs electrode (N_D=4.2—8.0×10^{18} cm^{-3}). The initial n-GaAs potential was −0.30 V and tip potential was +0.44 V.

As already shown in Fig. 4B, the anodic tunneling current was very easy to flow at this electrode of highest doping level (N_D=4.2—8.0×10^{18} cm^{-3}) in the reverse bias region. No current was, however, observed at the S-treated n-GaAs electrode even when the potential was as positive as +3.3 V.

Discussion

Qualitative Description for Tunneling Behavior of GaAs Electrodes in Electrolyte Solution. The i_T–V relations of GaAs electrodes can be explained by considering the potential dependent band bending of the semiconductor electrode and the relative positions of the Fermi levels of the tip and semiconductor. The energy diagrams for n-GaAs/solution/tip interface in different potential regions are shown in Fig. 3A to describe the i_T–V relation. The model is essentially the same as the one proposed to explain the TCV behavior of a semiconductor electrode.[27,38,40]

When the potential of n-GaAs electrode is more negative than the V_{fb}, the n-GaAs electrode is under "accumulation" condition and there are enough carriers (electrons) at the semiconductor surface. If the tip is brought close to the n-GaAs surface under this condition with feedback circuit active, electrons can tunnel from n-GaAs to the tip and the pre-set tunneling current flows. As the potential is swept positively in external control mode, the Fermi level of n-GaAs is lowered and the electron concentration at the n-GaAs surface is decreased, leading to a rapid decrease of the cathodic tunneling current tunneling from n-GaAs to the tip (Fig. 3A). The tunneling current decreases to zero near the V_{fb} and no current is expected to flow at potentials more positive than the V_{fb}, as observed experimentally, since a space charge layer is formed within the semiconductor when the potential becomes more positive than the V_{fb} ("depletion" region). The space charge layer can be considered as an extra barrier for the electron tunneling from n-GaAs to the tip. The tunneling barrier becomes thicker as reverse bias increases.

Anodic tunneling current was observed, however, as the potential became much more positive (>+2.5 V), although it was much smaller than the cathodic tunneling current observed in the forward bias region (Fig. 3A). As mentioned above, the space charge layer, which blocks the tunneling of electrons, becomes thicker in the potential region much more positive than the V_{fb}. The Fermi level of the semiconductor electrode, however, becomes lower than that of the tip under a very large reverse bias condition and the barrier for electron tunneling from the tip to the sample becomes thinner as potential becomes more positive. Thus, electrons are expected to tunnel from the tip to the unoccupied state of the conduction band in n-GaAs electrode in an opposite direction to that in forward bias region.

A larger anodic tunneling current was observed at an electrode of higher doping density (Fig. 4). This is reasonable, since a semiconductor of higher density has a thinner space charge layer at a given electrode potential. One must note, however, that an oxide layer may be formed on the n-GaAs surface at very positive potential and the nature of the n-GaAs surface should be changed by the formation of the

oxide layer. Thus, a quantitative treatment of the anodic tunneling current is rather difficult.

A similar qualitative interpretation can be given for the i_T–V relation of p-GaAs shown in Fig. 3B, except for the facts that the space charge layer is formed in the anodic potential region and holes are the majority carrier (see the energy diagrams in the figure). As described in the Results section, anodic current flowed in the forward bias region at p-GaAs electrode; therefore, the change of surface nature of p-GaAs during the ETS measurement should be larger than that of n-GaAs electrode.

Semi-Quantitative Analysis for the Tunneling Behavior of n-GaAs in the Forward Bias Region. Tunneling current for an s-wave-tip is often given approximately by:[7]

$$i_T \propto \rho_s(0, E_f)\cdot\Delta V\cdot\exp(-2\varkappa_0 x) \tag{6}$$

where $\rho_s(0,E_f)$ represents the sample surface LDOS near the Fermi level, E_f, ΔV and x are the bias and the distance between sample and tip and $\varkappa_0$ is the decay constant which is given by

$$\varkappa_0 = (2\pi/h)(2m\phi)^{1/2} \tag{7}$$

where h is the Planck constant, m is the mass of electron, and ϕ is the mean barrier height. Unfortunately, however, this equation is applicable only to the situation where ΔV is very small and, therefore, is not suitable for the analyses of the present results as the bias is more than few hundred mV.

The net flux of the tunneling electron from a substrate to a tip, J_T, can be given by:

$$J_T = J_{S\to T} - J_{T\to S}, \tag{8}$$

where $J_{S\to T}$ and $J_{T\to S}$ and the flux of the tunneling electron from the substrate to the tip and that from the tip to the substrate, respectively. When the bias between the substrate and the tip zero, no net tunneling current flows as

$$J_{S\to T} = J_{T\to S} = J_0, \tag{9}$$

where J_0 is the flux of tunneling electron flowing in both directions. A generalized expression was derived for the bias dependence of J_T for the electron tunneling between similar electrodes by Simmons for an arbitrary barrier by treating both $J_{S\to T}$ and $J_{T\to S}$.[48] He has shown that an expression similar to Eq. 6 can be deduced for the low bias limit. He further applied the formula for a rectangular barrier for low, intermediate and high bias cases. Here we modified his treatment so that it can be applied to the semiconductor/electrolyte/tip interface.

Figure 9A shows an energy diagram for n-GaAs/electrolyte/tip interface when n-GaAs and the tip are at V_{fb}, where E_c, E_v, and E_f are the energy of the conduction band, valence band, and the Fermi level, respectively, and ϕ_0 is the barrier height for electron tunneling. In the treatment of this study, E_c is assumed to be equal to E_f in the semiconductor bulk. In this case no net tunneling current flows as the bias is zero, although electron tunnel between n-GaAs and the tip in both directions with same rate, J_0. In this case, J_0 can be given by:

$$J_0 \propto \phi_0 \exp(-2\varkappa_0 x). \tag{10}$$

In this case, ϕ in Eq. 7 should be replaced by ϕ_0. When the tip potential is made more positive while keeping n-GaAs at the V_{fb} as shown in Fig. 9B, the mean barrier height for the electron tunneling from n-GaAs to the tip becomes ϕ_0', which is smaller than ϕ_0 by $[e(V_{fb}-V_{Tip})]/2$. On the other hand, the mean barrier height for the electron tunneling from the tip to n-GaAs becomes $\phi_0+[e(V_{fb}-V_{Tip})]/2$. Thus, J_T is given by

$$\begin{aligned} J_T &= J_{S\to T} - J_{T\to S} \\ &\propto \{\phi_0' \exp(-2\varkappa_{S\to T}x)\} - \{[\phi_0' + e(V_{fb}-V_{Tip})]\exp[-2\varkappa_{T\to S}x]\}, \end{aligned} \tag{11}$$

where

$$\varkappa_{S\to T} = (2\pi/h)(2m\phi_0')^{1/2}, \tag{12}$$

$$\varkappa_{T\to S} = (2\pi/h)\{2m[\phi_0' + e(V_{fb} - V_{Tip})]\}^{1/2}. \tag{13}$$

Since we consider only the situation of intermediate bias with the V_{fb} is more negative than V_{Tip} (Fig. 9), the absolute value of the second term in Eq. 11 is much smaller than the first term. Furthermore, there is no acceptor level for the electron tunneling from the tip to n-GaAs, because the Fermi level of the tip is within the forbidden band of n-GaAs. Thus, the second term can be ignored.

If the potential of n-GaAs electrode is made more negative than the flat band potential by $(V-V_{fb})$, the mean barrier height for the electron tunneling from n-GaAs to the tip decreases by $e(V_{fb}-V)$, but that for the electron tunneling from the tip to n-GaAs does not change (Fig. 9C). This is because the band edges of the conduction and valence bands of n-GaAs are pinned with respect to the vacuum level and the potential drop occurs solely within n-GaAs.[49] The second term of Eq. 11 can be ignored also in this case. Thus, Eq. 11 can be written for this situation as:

$$\begin{aligned} J_T &= J_{S\to T} - J_{T\to S} \\ &\approx J_{S\to T} \\ &\propto \{\phi_0' + e(V_{fb} - V)\}\exp(-2\varkappa_{S\to T}x), \end{aligned} \tag{14}$$

where

$$\varkappa_{S\to T} = (2\pi/h)\{2m[\phi_0' - e(V_{fb} - V)]\}^{1/2}. \tag{15}$$

In this treatment the tunneling current is considered to be affected by potential only through the potential dependence of the mean barrier height. Since the surface concentration of electrons varies with potential quite significantly in the present case, the potential dependence of the surface electron concentration should be taken into account and J_T should be given by:

$$J_T \propto n_s(V)\cdot\{\phi_0' - e(V_{fb} - V)\}\exp(-2\varkappa_{S\to T}x), \tag{16}$$

where $n_s(V)$ is the surface electron concentration at a given potential and is approximately given by:

$$n_s(V) = n_0 \exp[e(V_{fb} - V)/kT], \tag{17}$$

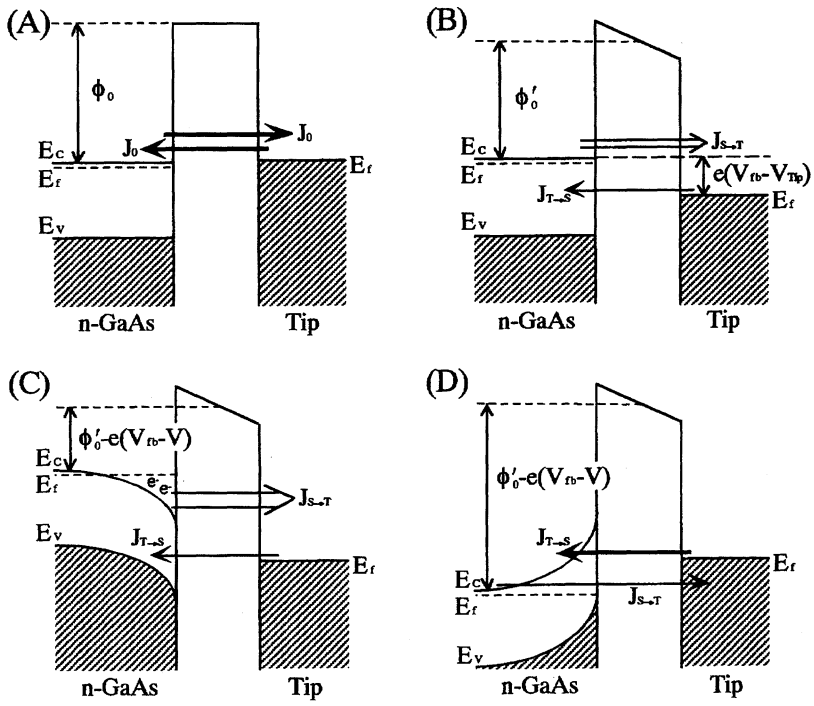

Fig. 9. Energy diagram of n-GaAs/solution/tip interface when the potential of (A) n-GaAs and the tip were at V_{fb}; (B) the tip was more positive than the V_{fb} while keeping n-GaAs at the V_{fb}; (C) n-GaAs was more negative and the tip was more positive than the V_{fb}; (D) n-GaAs was much more positive than the V_{fb}.

where n_0 is the electron concentration in the bulk of the n-type semiconductor ($n_0 \approx N_D$), k is the Boltzmann constant, and the V_{fb} and V are the flat band potential and the potential of the semiconductor electrode, respectively, with respect to a common reference electrode. Thus, Eq. 16 becomes

$$J_T \propto n_0 \exp[e(V_{fb} - V)/kT] \cdot \{\phi_0' - e(V_{fb} - V)\} \exp(-2\varkappa_{S\to T} x). \quad (18)$$

This equation suggests that the tunneling current changes exponentially with potential as long as the term $(V_{fb}-V)$ does not vary too much. Figure 10 is the replot of the results of Fig. 4A and shows the potential dependence of log of tunneling current for n-GaAs electrode of two different doping densities ($N_D = 0.84\times10^{18}$ cm^{-3} and 2.48×10^{18} cm^{-3}). It is clear that the tunneling current actually varies exponentially with potential, as expected from Eq. 18. The surface electron concentrations of the two samples are calculated by using Eq. 17 and are also plotted as a function of the potential in Fig. 10. The n-GaAs of higher doping density shows a higher surface electron concentration at a given potential but the slopes of log $(n_s(V))$–V relations are the same. The slopes of the log (i_T)–V relation for two samples are also very similar. However, the slopes of log $(n_s(V))$–V relations are larger than those of the log (i_T)–V relations. This discrepancy will be discussed more later.

Effects of the pre-set tunneling current on the tunneling behavior can be also explained, based on Eq. 18. If one starts the ETS measurement at the same initial sample potential with the different pre-set tunneling current (Fig. 5), the tip-sample distance is different and a smaller pre-set current

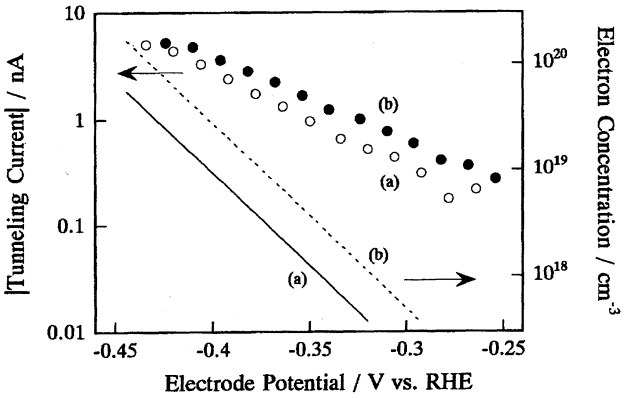

Fig. 10. log (i_T)–V relations of n-GaAs with doping levels of (a) 0.84×10^{18} cm^{-3} and (b) 2.48×10^{18} cm^{-3}. Results are of Fig. 4A. Surface electron concentration of n-GaAs electrode with the doping densities of (a) 0.84×10^{18} cm^{-3} and (b) 2.48×10^{18} cm^{-3} are also shown in the figure by solid and broken line, respectively.

means a larger tip-same distance, as Eq. 18 clearly shows. In the present ETS measurement, the distance between the tip and the sample was fixed after the STM internal feedback control mode was switched into the external control mode. Thus, the smaller the pre-set current, i.e., the larger the tip-sample distance, the smaller the tunneling current at a given bias. Under the experimental conditions of Fig. 5, the tunneling currents of the two different pre-set tunneling current at a given potential, V, are given by:

$$J_{T,1} \propto n_0 \exp[e(V_{fb} - V)/kT] \cdot \{\phi_0' - e(V_{fb} - V)\} \exp(-2\kappa_{S\to T} x_1), \quad (19)$$

$$J_{T,2} \propto n_0 \exp[e(V_{fb} - V)/kT] \cdot \{\phi_0' - e(V_{fb} - V)\} \exp(-2\kappa_{S\to T} x_2). \quad (20)$$

Thus, if one plots the $\log(i_{T,1})$ and $\log(i_{T,2})$ as a function of potential, the slopes should be the same. Experimental results confirmed this expectation, as shown in Fig. 11, where the results of Fig. 5A obtained for two different pre-set current are replotted as $\log(i_T)$–V relations. Straight lines are again observed and the slopes of the two curves are almost the same. This result supports the model that the potential dependence of the tunneling current is essentially explained by considering the surface electron concentration and the pre-set current affects only the tip-sample distance.

The effect of the sample-tip distance should be also considered in any discussion of the effect of initial sample potential. The tip should be closer to the sample when smaller initial bias is employed at a given pre-set tunneling current. Since the tip potential was fixed at +0.15 V in Fig. 6, the more negative the initial sample potential, the larger the initial bias and, therefore, the larger the tip-sample distance. Thus, the current should be smaller in this case, as observed experimentally (curve a, Fig. 6). The $\log(i_T)$–V relations of two different initial sample potentials are obtained by using the results of Fig. 6A and are shown in Fig. 12. As was the case for the effect of the pre-set current, two straight lines of almost the same slope were obtained, supporting the above model.

The effects of the tip potential on the tunneling behavior seem to be more complicated. The results of Fig. 7A are replotted as the potential dependence of $\log(i_T)$ in Fig. 13. Although linear relations are obtained in all the cases, the slopes of $\log(i_T)$–V relations depend on the tip potential. The more positive the tip potential was, the smaller the slope was. The potential dependence of the surface electron concentrations of n-GaAs of the same doping density is also shown in Fig. 10. Different tip potentials for a given sample potential and a given pre-set tunneling current means different initial bias, i.e., different tip-sample distance (Eq. 18). The results in Figs. 11 and 12 clearly show that the tip-sample distance does not affect the slope of $\log(i_T)$–V relation, as expected from Eq. 18.

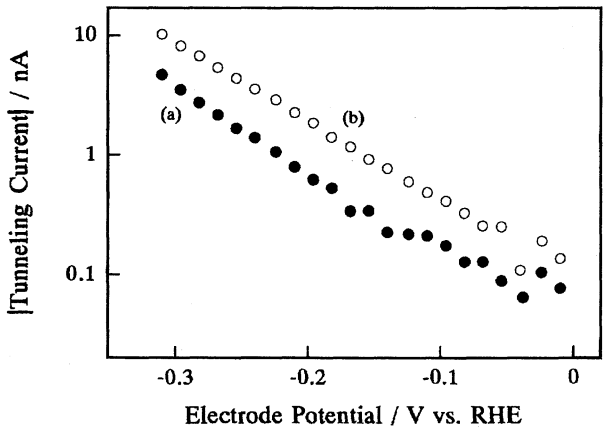

Fig. 11. $\log(i_T)$–V relations for two different pre-set tunneling currents of (a) −4.5 nA and (b) −10 nA. Results are of Fig. 5A.

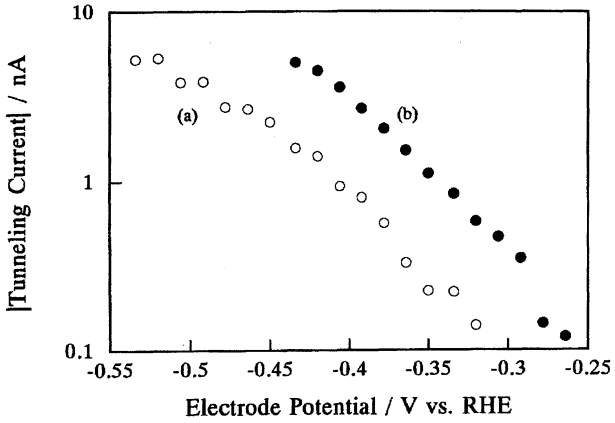

Fig. 12. $\log(i_T)$–V relations for two different initial sample potentials of (a) −0.55 V and (b) −0.45 V. Results are of Fig. 6A.

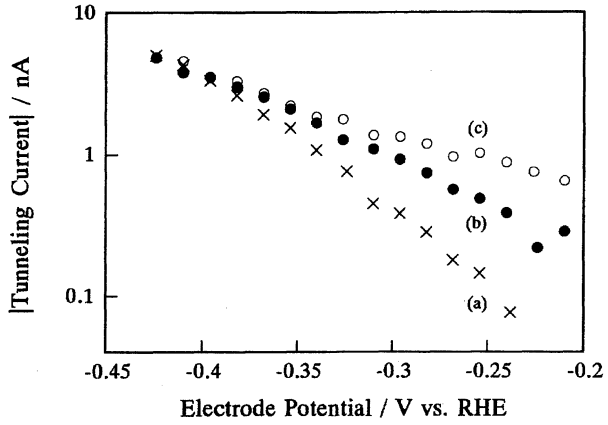

Fig. 13. $\log(i_T)$–V relations for three tip potentials of (a) +0.16 V, (b) +0.36 V, and (c) +0.56 V.

The different tip-potential means the different mean barrier height, since ϕ_0' is given by:

$$\phi_0' = \phi_0 - [e(V_{fb} - V_{Tip})]/2. \quad (21)$$

The potential dependence of $\log(i_T)$ was estimated using Eq. 18 by taking Eq. 21 into account. Calculated results show that $\log(i_T)$–V relations are almost linear even if all the terms in Eq. 18 are taken into account, but V_{Tip} affects the slope only slightly. Thus, the mean barrier height difference cannot explain the discrepancy between the slopes of $\log(n_s(V))$–V relations and that of $\log(i_T)$–V relations as well as the tip-potential dependent slope in $\log(i_T)$–V relations.

We have assumed so far that all the potential drop occurs within the n-GaAs electrode, but it is known that some of the potential drop occurs also in the Helmholtz layer when the carrier density or the surface state density is high.[49] This makes the slope of $\log(n_s(V))$–V and, therefore, of $\log(i_T)$–V

relations small. This should be at least a part of the reasons for the discrepancy between the slopes of $\log(n_s(V))$–V relations and that of $\log(i_T)$–V relations. The tip-potential dependent slope suggests that the presence of the tip near the semiconductor electrode affects the potential distribution at the semiconductor/electrolyte interface.

Semi-Quantitative Analysis for the Tunneling Behavior of n-GaAs in Very Positive Potential Region. As discussed before, when the potential of n-GaAs became very positive, a small amount of tunneling current flowed from the tip to n-GaAs electrode. The energy diagram for this situation is shown in Fig. 9D. Again, the barrier shape at the interface does not change if one assumes all potential drops within the semiconductor. In this case, however, in addition to the tunneling barrier at n-GaAs/electrolyte/tip interface in the forward bias region discussed above, the space charge layer formed within n-GaAs electrode should be considered as an extra barrier for electron tunneling from the tip to the conduction band. It is obvious from Fig. 9D that the second term dominates in Eq. 8, as $(V-V_{Tip})$ is fairly large and there is no vacant state in the tip at E_f of n-GaAs in the present condition.

The effects of the pre-set tunneling current and the initial sample potential on the tunneling current at a given potential can be analyzed simply as a result of the different sample-tip distance, as was the case in the forward bias region. Thus, the larger the pre-set tunneling current, the smaller the tip-sample distance and, therefore, the larger the tunneling current in the reverse bias region (Fig. 5B). Similarly, the more negative the initial sample potential, the larger the tip-sample distance and, therefore, the smaller the tunneling current in the reverse bias region (Fig. 6B).

As described above, the space charge layer formed within n-GaAs in the reverse bias region acts as an extra barrier for the electron tunneling from the tip to n-GaAs. The thickness and the height of the space charge layer affects the tunneling probability in the reverse bias region. The degree of the tunneling process through the extra barrier (space charge layer) can be evaluated by calculating a transmission coefficient through the barrier. The potential distribution within the semiconductor can be calculated by solving the Poisson equation, which can be written for the present situation as:

$$d^2V(x)/dx^2 = eN_D/\varepsilon_0\varepsilon, \qquad (22)$$

where $V(x)$ is the potential of the semiconductor at x from the semiconductor surface, ε_0 is the dielectric constant of vacuum, ε is the relative dielectric constant of the semiconductor, and N_D is the concentration of the donors.[50] One must note $V(0)=V_{fb}$ and $V(\infty)=V$. As an example, the energy diagrams of the conduction band of n-GaAs of two doping densities ($N_D=0.84\times10^{18}$ cm^{-3}, dotted line; 2.48×10^{18} cm^{-3}, solid line) were calculated for $V=+3.16$ V by using Eq. 22 with $V_{fb}=-0.34$ V. Results are shown in Fig. 14A. The tip potentials of +0.16 V, +0.36 V, and +0.56 V which were employed in the present study are also indicated in the figure. The energy diagrams were enlarged for the region near the Fermi level of the tip in Fig. 14B. Figure 14 clearly shows that n-GaAs of higher doping density has a thinner space charge layer at a given tip potential. The transmission coefficient through the space charge layer for the electron tunneling from the tip to the conduction band of n-GaAs, k_t, depends on the thickness of the space charge layer at the energy of the E_f of the tip, $d(V_{Tip})$, and the energy difference between the E_f of the tip and bottom of the conduction band at the surface, which is equal to $e(V_{Tip}-V_{fb})$. The following Gamaw–Jeffreys equation can be used for the calculation of k_t:[51]

$$k_t = \exp\{(8\pi d(V_{Tip})/3h)[2me(V_{Tip}-V_{fb})]\}. \qquad (23)$$

Here the barrier shape was assumed to be a triangle as a first approximation. This assumption is reasonable, as shown in Fig. 14B.

The values of k_t were calculated by using Eq. 23 with the values of the thickness of the space charge layer for various tip potentials shown in Fig. 14 for $V=+3.16$ V. The calculated values for the two doping densities are shown in Fig. 15

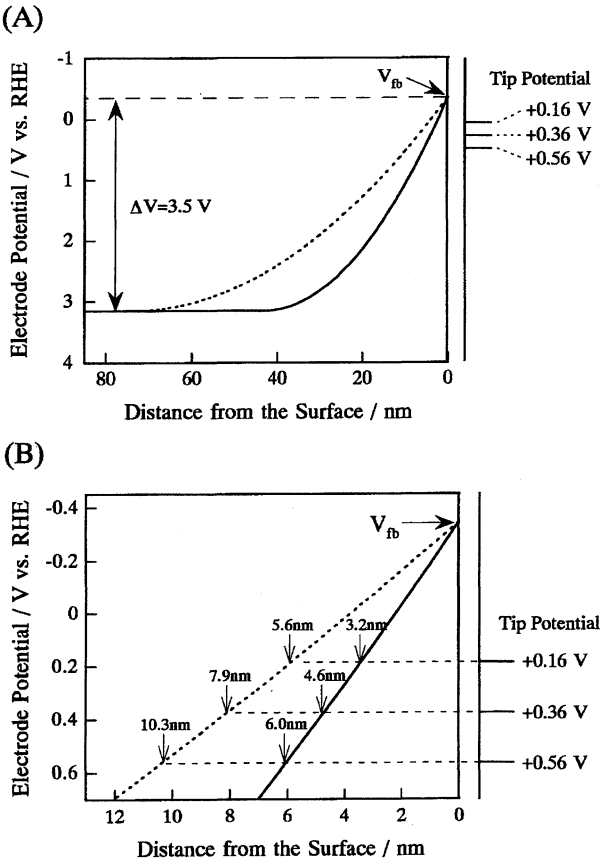

Fig. 14. Calculated conduction band position as a function of distance in the space charge region of n-GaAs/solution/tip interface for $N_D=2.48\times10^{18}$ cm^{-3} (solid line) and $N_D=0.84\times10^{18}$ cm^{-3} (dotted line). (A) whole region; (B) enlarged region near interface. $V_{fb}=-0.34$ V, $\Delta V=3.50$ V. The thickness of space charge layer for respective tip potential of (a) +0.16 V, (b) +0.36 V, and (c) +0.56 V were shown at the figure. See text for details.

as a function of the tip potential. The higher the doping density, the larger the k_t, since the barrier width is thinner. This result is in agreement with the experimental results (Fig. 4), although the calculated effect of doping density on k_t is much larger than the experimentally observed effect on i_T. Figure 15 shows that k_t for $N_D=2.48\times10^{18}$ cm^{-3} is 10^5 times larger than that for $N_D=0.84\times10^{18}$ cm^{-3} in the case of a tip potential of +0.16 V. Although a similar tendency of doping density dependence was obtained for i_T, the effect was less significant, as i_T at n-GaAs of $N_D=2.48\times10^{18}$ cm^{-3} was only about 4 times larger than that of $N_D=0.84\times10^{18}$ cm^{-3} at the same experimental conditions (Fig. 4B).

Figure 15 also shows that k_t increases as the tip potential becomes more negative. The dependencies of log (i_T) and log (k_t) on n-GaAs potential in very positive potential region are shown for three different tip potentials in Fig. 16. The tunneling current in very positive potential region was found to flow more easily at a more positive sample potential and with a more negative tip potential (Fig. 7B and Fig. 16A) and the calculated relation between log (k_t) and the potential of n-GaAs at different tip potentials showed a similar tendency (Fig. 16B). The values of k_t depended on the potential of n-GaAs and on the tip potential more significantly than those of i_T. For example, i_T of n-GaAs at +3 V increased ca. one order of magnitude by changing the tip potential from +0.56 V to +0.16 V (Fig. 7B) but k_t increased more than ten orders of magnitude for the same change (Fig. 16B). Similarly, the tunneling current increased about 5 times as the potential changed from +2 V to +3 V with a given tip potential of +0.16 V (Fig. 6B) while the calculated k_t is expected to increase ca. 30 times under the same conditions (Fig. 16B). The effect of the tip potential on the tunneling current can be explained by considering the thickness of the space charge layer at the energy of tunneling electron, i.e., the Fermi level of the tip. As the thickness of the tunneling barrier within the space charge layer is thinner when the tip potential is more negative (Fig. 14), the tunneling probability

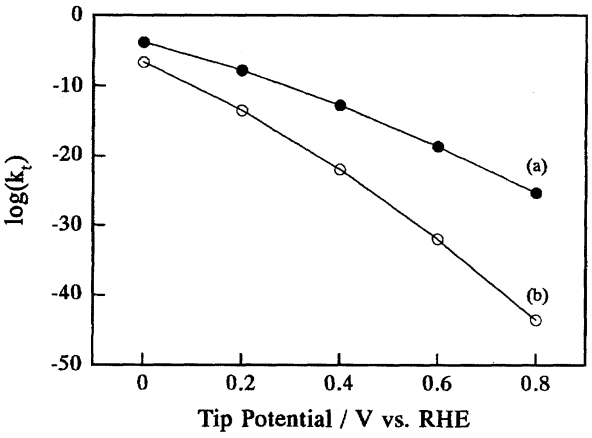

Fig. 15. Calculated transmission coefficients were shown as a function of the tip potential for (a) $N_D=2.48\times10^{18}$ cm^{-3} and (b) $N_D=0.84\times10^{18}$ cm^{-3}. $V_{fb}=-0.34$ V and n-GaAs potential=+3.1 V.

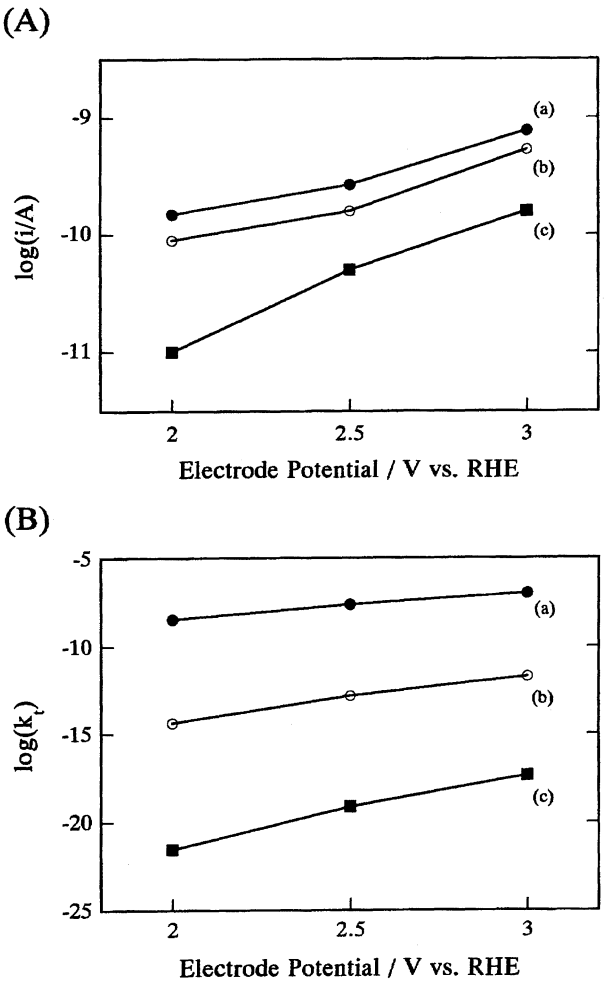

Fig. 16. (A) log i and (B) calculated transmission coefficients as a function of substrate potential at n-GaAs electrode ($N_D=2.48\times10^{18}$ cm^{-3}) the tip potential of (a) +0.16 V, (b) +0.36 V, and (c) +0.56 V.

from the tip to n-GaAs electrode through the space charge layer should be higher at more negative tip potential, i.e., at higher energy. As the potential becomes more positive, the difference between the V_{fb} and V increases, leading to the decrease of the thickness of the space charge layer at the tip potential $d(V_{Tip})$ and, therefore, the increase of k_t.

Several reasons should be considered for the discrepancy between the potential dependence of k_t and that of i_T. One important reason is that the tunneling barrier consists of not only the space charge layer of n-GaAs but also the barrier between the n-GaAs surface and the tip, which is considered to be the only barrier for the electron tunneling in forward bias region in the preceding section. Thus, the potential dependence of k_t is not necessarily that of i_T.

A more important reason seems to be, however, the existence of some surface states and impurity levels of n-GaAs. If one looks at the energy diagram shown in Fig. 14, the thickness of the space charge layer at the tip potential $d(V_{Tip})$ is far too thick for electron tunneling to take place with reasonable tunneling probability without considering the resonance tun-

neling through these states. The importance of the surface states to the tunneling behavior is clearly demonstrated in Fig. 8. The anodic tunneling current flowed more easily at an n-GaAs electrode treated with Ru than at the etched GaAs electrode (Fig. 8A) but the S-treated n-GaAs electrode behaved as an ideal semiconductor and tunneling current was observed only in the "accumulation" region (Fig. 8B). The Ru- and S-treatments have been known to increase and decrease, respectively, the surface state density.[24,26,46,47] These results confirmed those obtained by the tip-current voltammetry (TCV) measurement reported before.[43]

Comparison between the Results of ETS and TCV. Finally, the results of ETS should be compared with those obtained by TCV.[40—43] Although essential features are similar, there are several important differences to be noted. The tip currents which flowed in weak depletion region and in very positive potential region in the case of TCV were much larger than those observed in the present ETS measurements. In the case of TCV measurement, the feedback circuit of the STM instrument functions all the time. When the tunneling current becomes smaller than the pre-set current, the feedback circuit forces the tip-sample distance to become small so that the pre-set current can flow. Of course, there is a situation when the tip current is smaller than the pre-set current even if the tip touches the surface. The current observed in this situation is not the tunneling current but the current at a Schottky junction. As the potential becomes much more positive, the tip current begins to increase and finally reaches the pre-set current. Then the tip is removed from the semiconductor electrode surface.

On the other hand, in the case of ETS measurement, the feedback loop of STM does not work and the piezo voltage of the tip controlled by an external D/A converter keeps the tip-sample distance constant during the experiment. Tunneling current decreases continuously with decreasing forward bias and becomes zero at potential of the V_{fb}. As the potential becomes positive enough, the tunneling current is able to flow from the tip to n-GaAs electrode. Thus, the tip-sample distance in the ETS measurements should be larger than that in the TCV measurement in the depletion condition.

Conclusion

An electrochemical tunneling spectroscopy (ETS) system was constructed and applied for n-GaAs and p-GaAs single crystal electrodes. The effects of doping density, tip/sample potential, and present current/potential as well as the surface treatment on the tunneling current–electrode potential relations were investigated in detail. In the forward bias region, the tunneling current decreased quickly as the potential became close to the flat band potential. This was attributed to the decrease of the concentration of surface majority carriers of GaAs electrode.

Since the space charge layer worked as an extra barrier to block the tunneling process, no current can be expected in the reverse bias region. However, as the reverse bias became very high, a small current flowed in the direction opposite to that in forward bias region. The doping level, the tip-sample distance, the tip potential, and the surface treatment by ruthenium and sulfur were found to affect the behavior in the reverse bias region significantly.

The tunneling behaviors in the forward and reverse bias regions were discussed semi-quantitatively, based on the calculation of surface electron concentration and the transmission coefficient through the space charge barrier, respectively. The agreement between the calculated and experimental results was fair and various reasons for the discrepancies were considered. All the results and the comparison with the TCV confirmed the importance of the ETS in the study of electronic structure of semiconductor electrode.

This work was partially supported by Grant-in-Aids for Scientific Research No. 06740428 and for Priority Area Research Nos. 0545202, 0645202, and 0745202 from the Ministry of Education, Science, Sports and Culture.

References

1) G. Binnig, H. Rohrer, Ch. Gerber, and E. Weibel, *Appl. Phys. Lett.*, **40**, 178 (1982).
2) G. Binnig, H. Rohrer, Ch. Gerber, and E. Weibel, *Phys. Rev. Lett.*, **49**, 57 (1982).
3) "Scanning Tunneling Microscopy I, II," ed by R. Wiesendanger and H. J. Guntherodt, Springer-Verlag, Berlin (1992).
4) "Scanning Tunneling Microscopy and Spectroscopy, Theory, Techniques and Applications," ed by D. A. Bonnell, VCH, New York (1993).
5) C. J. Chen, "Introduction to Scanning Tunneling Microscopy," Oxford University Press, New York (1993).
6) D. R. Lonber and B. A. Parkinson, *Anal. Chem.*, **66**, 84R (1994).
7) "Nanoscale Probes of the Solid/Liquid Interface," ed by A. A. Gewirth and H. Siegenthaler, Kluwer Academic Publishers, Dordrecht (1995).
8) R. Hamers, R. Tromp, and J. Demuth, *Phys. Rev. Lett.*, **56**, 1972 (1986).
9) R. Tromp, R. Hamers, and J. Demuth, *Phys. Rev.*, **B34**, 1388 (1986).
10) N. Garcia, *IBM J. Res. Dev.*, **30**, 533 (1986).
11) J. H. Coombs and J. B. Pethica, *IBM J. Res. Dev.*, **30**, 455 (1986).
12) J. K. Gimzewski, R. Moller, D. W. Pohl, and R. R. Schlittler, *Surf. Sci.*, **39**, 15 (1987).
13) R. M. Feenstra, J. A. S. Stroscio, and A. P. Fein, *Surf. Sci.*, **181**, 295 (1987).
14) J. Kirtley, S. Raider, R. Feenstra, and A. P. Fein, *Appl. Phys. Lett.*, **50**, 1607 (1987).
15) H. Hess, R. Robinson, R. Dynes, J. Valles, and J. Waszczak, *Phys. Rev. Lett.*, **62**, 214 (1989).
16) Y. Kuk and P. J. Silverman, *J. Vac. Sci. Technol.*, **A8**, 289 (1990).
17) R. M. Feenstra, *Surf. Sci.*, **299/300**, 965 (1994).
18) F-R. F. Fan and A. J. Bard, *J. Phys. Chem.*, **95**, 1969 (1991).
19) N. Casillas, S. R. Snyder, W. H. Smyrl, and H. S. White, *J. Phys. Chem.*, **95**, 7002 (1991).
20) J. A. Stroscio, R. M. Feenstra, D. M. Newns, and A. P. Fein, *J. Vac. Sci. Technol.*, **A6**, 499 (1988).

21) F-R. F. Fan and A. J. Bard, *J. Phys. Chem.*, **97**, 1431 (1993).
22) S. P. Kelty, A. F. Ruppert, R. R. Chianelli, J. Ren, and M.-H. Whangbo, *J. Am. Chem. Soc.*, **116**, 7857 (1994).
23) Yu. V. Pleskov and Yu. Grevich, "Semiconductor Photoelectrochemistry," Plenum Press, New York (1986).
24) K. Uosaki, Y. Shigematsu, S. Kaneko, and H. Kita, *J. Phys. Chem.*, **93**, 6521 (1989).
25) K. Uosaki and H. Kita, *J. Phys. Chem.*, **88**, 4197 (1984).
26) S. Kaneko, K. Uosaki, and H. Kita, *J. Phys. Chem.*, **90**, 6654 (1986).
27) K. Uosaki and H. Kita, *J. Am. Chem. Soc.*, **108**, 4294 (1986).
28) K. Itaya, R. Sugawara, Y. Morita, and H. Tokumoto, *Appl. Phys. Lett.*, **60**, 2534 (1992).
29) S.-L. Yau, K. Kaji, and K. Itaya, *Appl. Phys. Lett.*, **66**, 766 (1995).
30) S.-L. Yau. F. F. Fun, and A. J. Bard, *J. Electrochem. Soc.*, **139**, 2825 (1992).
31) P. Allongue, V. Kieling, and H. Gerischer, *J. Electrochem. Soc.*, **140**, 1009 (1993).
32) K. D. Kepler and A. A. Gewirth, *Surf. Sci.*, **303**, 101 (1994).
33) K. Uosaki and M. Koinuma, *J. Electroanal. Chem.*, **357**, 301 (1993).
34) M. Koinuma and K. Uosaki, *Surf. Sci.*, **311**, L737 (1994).
35) H. Yao, S.-L, Yau, and K. Itaya, *Surf. Sci.*, **335**, 166 (1995).
36) J. Wiechers, T. Twomey, D. M. Kolb, and R. J. Behm, *J. Electroanal. Chem.*, **248**, 451 (1988).
37) J. Pan, T. W. Jing, and S. M. Lindsay, *J. Phys. Chem.*, **98**, 4205 (1994).
38) K. Itaya and E. Tomita, *Chem. Lett.*, **1989**, 285.
39) K. Itaya and E. Tomita, *Surf. Sci.*, **219**, L515 (1989).
40) P. Carlsson, B. Holmström, H. Kita, and K. Uosaki, *Surf. Sci.*, **237**, 280 (1990).
41) P. Carlsson, B. Holmström, H. Kita, and K. Uosaki, *J. Electroanal. Chem.*, **283**, 425 (1990).
42) S. Eriksson, P. Carlsson, B. Holmström, and K. Uosaki, *J. Electroanal. Chem.*, **313**, 121 (1991).
43) K. Uosaki and M. Koinuma, *Faraday Discuss. Chem. Soc.*, **94**, 361 (1992).
44) J. F. Fan, H. Oigawa, and Y. Nannichi, *Jpn. J. Appl. Phys.*, **27**, L1331 (1988); B. J. Skromme, C. J. Sandroff, E. Yablonoitch, and T. Gemitter, *Appl. Phys. Lett.*, **51**, 2022 (1987).
45) "NanoScope I Instruction Manual, Version 1.1," Digital Instruments Inc.
46) K. Uosaki and H. Kita, *J. Electroanal. Chem.*, **259**, 301 (1989).
47) K. Uosaki and H. Kita, *Chem. Lett.*, **1984**, 953.
48) J. G. Simmons, *J. Appl. Phys.*, **34**, 1793 (1963).
49) K. Uosaki and H. Kita, "Modern Aspects of Electrochemistry," ed by R. E. White, J. O'M. Bockris, and B. E. Conway, Plenum Press, New York (1986), Vol. 18, p. 1.
50) V. A. Myamlin and Yu. V. Pleskov, "Electrochemistry of Semiconductors," Plenum Press, New York (1967).
51) J. O'M. Bockris and S. U. M. Khan, "Quantum Electrochemistry," Plenum Press, New York (1979), p. 249.